

Abstract

Burkholderia vietnamiensis is a Gram-negative, pathogenic bacteria commonly implicated in cystic fibrosis-associated infections. Here, we investigate the crystal structures of a *B. vietnamiensis* Short-chain Dehydrogenase/Reductase (SDR), thought to be involved in the energetic or lipid biosynthetic pathways. In this analysis, we look at the overall structure, homolog alignments, and ligand binding interactions. Through these characterizations, we demonstrate that this SDR is a robust target for antibiotic drug development.

1. Introduction

The *Burkholderia* genus was originally classified in 1992; since then, there has been an explosion in the number of species discovered and classified (Lipuma, 2010). However, even though there have been numerous new *Burkholderia* species discovered, most research has focused on *B. Cepacia*. There has been little research to further characterize *B. vietnamiensis*.

There are essentially two categories of *Burkholderia* species: the non-pathogenic, and the pathogenic, which are often called Bcc. The Bcc grouping derives its name from *B. cepacia*, which is the most prominent and well studied of the pathogenic species (Mahenthiralingam *et al.*, 2005). The species that our structure was isolated from, *Burkholderia vietnamiensis*, falls into the Bcc grouping. These pathogenic *Burkholderia* are responsible for any number of human infections, most notably they are one of the common causes of pulmonary infections in patients that present with Cystic Fibrosis (CF) (Cystic Fibrosis Foundation, 2018). Patients with CF are unable to clear mucus from internal organs, particularly in the lungs, leading to a build-up that traps bacteria like *Burkholderia* (Scoffone *et al.*, 2017). The bacteria thrive in the warm, moist environment, often forming recalcitrant biofilms. Ultimately, this causes recurrent infections that contribute to the progressive nature of CF. Preventing, or limiting, the pathogenesis of *Burkholderia* in these patients presents an interesting pathway to prevent negative symptoms of the disease.

Recently, there has been a decline in antibiotic drug discovery paired with an increase in resistant bacteria, so it is imperative that work is done to develop effective new treatments (Lewis, 2013). Unfortunately, many Bcc *Burkholderia*, including *B. vietnamiensis*, are highly resistant to antibiotic therapies as evidenced by the presence of several beta-lactamases (Poirel *et al.*, 2009). However, it has been reported that *B. vietnamiensis* are still vulnerable to several of the aminoglycosides (Jassem *et al.*, 2011).

We present the crystal structures, PDB 5IDX and 5IDY, of a Short-chain Dehydrogenase/Reductase (SDR) from *B. vietnamiensis*. The SDR class of enzymes is very large, and they are typically NAD(P)(H)-dependent (Kavanagh *et al.*, 2008). These enzymes perform a wide variety of functions, serving as oxidoreductases for amino acids, sugars, and lipids in any number of biosynthetic processes (Kavanagh *et al.*, 2008). Using its similarities to homologous structures, we postulate that the SDR is involved in lipid biosynthesis or the degradation of ketone bodies for energy, both pathways being strong targets for antibiotic treatments.

3.1 Overall Structure

The crystal structures of both the apo (5IDX) and ligand bound (5IDY) of a short-chain dehydrogenase/reductase (SDR) from *Burkholderia vietnamiensis* have been determined at

resolutions of 1.95 Å and 1.85 Å, respectively. **Figure 1A** demonstrates the homodimeric asymmetric unit of 5IDX where each chain is 267 residues in length. While the asymmetric unit is a homodimer, we propose that the biologic unit is a homotetramer consisting of two asymmetric units arranged to yield dihedral, D₂, symmetry as shown in **figure 1B**. This symmetry is further seen in the 90° rotation shown in **figure 1C**. Each chain is represented in a different color (blue, green, purple, and yellow), and each chain is shown in complex with its natural ligand, NADP⁺ (red).

The biologic unit was determined using jsPISA analysis and the resultant structure was compared to similar SDRs from different genera that were identified using the Dali server.

First, we performed a buried surface area analysis based on the proposed homotetrameric biologic unit. The area of each of the four monomers was calculated, chain A = 4,136.3 Å², chain B = 4,174.7 Å², chain C = 4,136.6 Å², chain D = 4,178.6 Å². Next, the individual buried surface area of all interfaces was totaled at 1,194.8 Å², and the total surface area of the tetramer was consequently calculated as 15,431.4 Å². For reference, the buried surface area is 7.74% of the total surface area of the complex.

Second, electrostatic calculations were performed to generate an electrostatic potential map for a single monomer (**figure 2A**) (Dolinsky *et al.*, 2004). As shown on this electrostatic potential map, the NADP⁺ binding pocket is electropositive, as expected for the binding of an electron-rich ligand like NADP⁺. For simplicity, **figure 2A** only shows a single monomer; however, each monomer has its own NADP⁺ binding pocket.

Third, we analyzed the hydrophobicity of the interfaces between the four monomers. Due to the hydrophobic effect and the fact that SDRs are globular proteins, we expect that hydrophobic residues are preferentially buried along the monomer interfaces. As indicated in **figure 2BC**, residues lining the interfaces between all four monomers are largely hydrophobic, and only residues towards the periphery of the interfaces are hydrophilic.

To further investigate this tetrameric structure, jsPISA was used to determine any hydrogen bonding or salt bridge interactions stabilizing the interfaces. A total of thirty-nine intermonomer hydrogen bonds and salt bridges were found by jsPISA (Kriszenel, 2015).

Combining these results, we confirm the proposed tetrameric biologic unit.

3.2 Identification of Homologous Structures

As previously mentioned, 5IDX and 5IDY were compared to the structures of several other homologs identified using Dali, these structural comparisons are summarized in **figure 3** (Holm & Laakso, 2016). The resulting alignment of these structures shows the three-layer(αβα) sandwich structure of the chain, and the Rossmann fold of the NAD(P)(H) binding pocket, are conserved across genera (Dawson *et al.*, 2017). This does not come as a surprise, as SDRs are abundant in the RCSB. The wide variety of reactions catalyzed by SDRs is thought to have come about through the divergent evolution of an ancestral nucleotide binding domain. This divergence has subsequently resulted in the specialized function of the enzymes as they have picked up substrate-specific domains (Kavanagh *et al.*, 2008).

While the exact pathway our protein is involved in has not yet been reported, we hypothesize that it is involved in the synthesis and/or degradation of lipids and ketone bodies because of the high similarity to enzymes that perform similar functions in other organisms.

3.3 Ligand Binding Induced Conformational Changes

Next, we turned our focus to the differences between the ligand-unbound form, 5IDX, and the ligand-bound form, 5IDY. For the remainder of this discussion, we will only be looking at one chain of this SDR, as all conformational changes in one subunit are symmetric to the other subunits. As demonstrated by the C α alignment of 5IDX chain A (blue) and 5IDY chain A (lightblue) in **figure 3A**, there are no major triggered conformational changes upon NADP $^{+}$ binding.

However, in **figure 3BC**, we demonstrate changes in the positions and orientation of the amino acid side chains and backbone segments surrounding the nucleotide binding pocket. Side chains and backbone sections shown represent conformational changes great than 1 Å. These residues will be discussed in greater detail below in the context of ligand specificity.

3.4 Ligand Specificity

The SDR family has been characterized to bind with either NAD $^{+}$ or NADP $^{+}$. While NADP $^{+}$ is the natural substrate for this enzyme, we analyze the NADP $^{+}$ specificity and how it might compare to NAD $^{+}$, which has a similar structure.

First, we identified the specific residues involved in NADP $^{+}$ binding in the 5IDY structure (**figure 5A**). We see that there are 15 hydrogen bonds between the NADP $^{+}$ and the backbone and side chains of binding pocket residues that were in the range of 2.7-3.3 Å.

Next, in **figure 5BC**, the electrostatic potential surface was calculated and overlaid on the binding pocket where we have modeled both NADP $^{+}$ and NAD $^{+}$ (Dolinsky *et al.*, 2004). In **figure 5B**, we see the 2' phosphate of the NADP $^{+}$ nestled into the blue electropositive region of the binding pocket. In **figure 5C**, we see that when NAD $^{+}$ is modeled, there is an open cavity in the binding pocket and a loss of 4 hydrogen bonding interactions. While there is still a biochemically relevant number of binding interactions, this loss of 4 hydrogen bonds will clearly lead to an increase in K_d for NAD $^{+}$ when compared to NADP $^{+}$. This indicates that NADP $^{+}$ will bind with a higher affinity to the pocket than NAD $^{+}$.

3.5 Antibiotic Target Potential

Knowing that *Burkholderia* are highly resistant Gram-negative bacteria with high mortality rates from their related diseases, targeting key enzymes in their metabolic processes present robust opportunities for antibiotic drug discovery (Jassem, 2011). While the specific biochemical pathway for this SDR has not been identified, we have several key pieces of information indicating that limiting flux through this enzyme would potentially prove to be an effective way to target these bacteria. If we consider the specificity of the enzyme for NADP $^{+}$, a cofactor primarily used in anabolic processes like lipid synthesis, if we were to cut this off, the ability of the organism to grow and divide would likely slow. In recent years, lipid biosynthesis pathways have garnered increased interest as antibiotics targeting other pathways have either become ineffective, or their development has slowed (Parsons, 2011). Additionally, knowing that *Burkholderia* produce poly- β -hydroxybutyrate, and enzymes similar to this SDR are involved in

its metabolism, we postulate that if this SDR is inhibited, the organism's energy supply chain could be compromised (Zhu *et al.*, 2009). Thus, this would also limit the viability of the organism. Lead compounds for inhibiting this SDR could be designed on scaffolds already used to inhibit other SDRs, and SAR studies could be performed to exploit other interactions in the binding pocket that are specific to this enzyme.

4. Conclusion

Using the presented structures of this SDR from *Burkholderia vietnamiensis* we have a good understanding of the structure and can speculate on the specific function of this protein. As *Burkholderia* is known to be highly resistant, speculated to potentially be a biowarfare agent, and implicated in cystic fibrosis infections, we hypothesize that this SDR is a prime target for rational antibiotic design (Woods, 2006). The binding mechanism of NADP⁺ is well characterized, which could aid in developing novel inhibitors to combat these issues. Further biochemical characterization will be needed to definitively determine the exact substrate, which is of paramount importance if this protein is to instead be targeted by inhibitors to substrate binding.

References

- Cystic Fibrosis Foundation (2018). *Burkholderia Cepacia Complex*, <https://www.cff.org/Life-With-CF/Daily-Life/Germs-and-Staying-Healthy/What-Are-Germs/Burkholderia-Cepacia-Complex/>
- Dawson, N.L., Lewis, T. E., Das, S., Lees, J. G., Lee, D., Ashford, P., Orengo, C. A., Sillitoe, I. CATH: an expanded resource to predict protein function through structure and sequence. (2017). *Nucleic Acids Res.* **45(D1)**, D289-D295.
- Dolinsky, T. J., Nielsen, J. E., McCammon, J.A., Baker, N.A. (2004). *Nucleic Acids Research*. **32**, W665-W667
- Holm, L., Laakso, L. M. (2016) Dali server update. *Nucleic acids research* 44 (W1), W351-W355.
- Jassem, A. N., Zlosnik, J. E. A., Henry, D. A., Hancock, R. E. W., Ernst, R. K., Speert., D. P. (2011). *Antimicrobial Agents and Chemotherapy*. **55(5)**, 2256-2264
- Kavanagh, K. L., Jörnvall, H., Persson, B., Oppermann, U. (2008). *Cell Mol Life Sci.* **65(24)**, 3895-906
- Krissinel, E. (2015). *Nucl. Acids Res.* **43(W1)**, W314-9
- Kubota, K., Nagata, K., Okai, M., Miyazono, K., Soemphol, W., Ohtsuka, J., Yamamura, A., Saichana, N., Toyama, H., Matsushita, K., Tanokura, M. (2011). *J. Mol. Biol.*, **407**, 543-555
- Levis, K., (2013). *Nature Reviews Drug Discovery*. **12**, 371–387
- Lipuma, J. J. (2010). *Clinical Microbiology Review*. **2**, 299-323
- Mahenthiralingam, E., Urban, T. A., Goldberg, J. B. (2005). *Nature Reviews Microbiology*. **3**, 144–156
- Paithankar, K. S., Feller, C., Kuettner, E. B., Keim, A., Grunow, M., Strater, N. (2007). *Febs J.* **274(21)**, 5767-5779
- Parsons, J. B., Rock, C. O. (2011). *Current opinion in microbiology*, **14(5)**, 544-549.
- PDB ID: 1O5I. Joint Center for Structural Genomics (JCSG). (2003). The structure 3-oxoacyl-(acyl carrier protein) reductase from *T. maritima*
- Poirel, L., Rodriguez-Martinez, J., Plésiat, P., Nordmann, P., (2009). *Antimicrobial Agents and Chemotherapy*. **53(3)**, 876-882

Rajavel, M., Perinbam, K. & Gopal, B. (2013). *Acta Cryst.* **D69**, 324-332.

Scoffone, V. C., Chiarelli, L. R., Trespidi, G., Mentasti, M., Riccardi, G., & Buroni, S. (2017). *Frontiers in microbiology*. **8**, 1592

The PyMOL Molecular Graphics System, Version 2.2 Schrödinger, LLC.

Woods D.E., Sokol P.A. (2006). The Genus Burkholderia. In: Dworkin M., Falkow S., Rosenberg E., Schleifer KH., Stackebrandt E. (eds) *The Prokaryotes*. Springer, New York, NY

Zhu, C. , Nomura, C. T., Perrotta, J. A., Stipanovic, A. J. and Nakas, J. P. (2010). *Biotechnol Progress*, **26**: 424-430.

Figure Captions

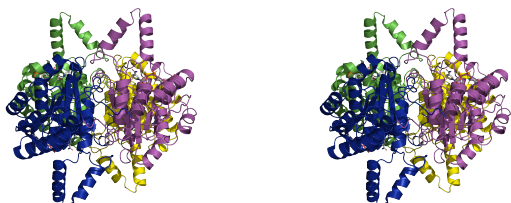


Figure 1: Crystal structure 5IDY of a short-chain dehydrogenase/reductase (SDR) from *Burkholderia vietnamiensis* determined at 1.95 Å resolution. Each chain (blue, carbon, magenta, and yellow), is in complex with NADP⁺ (red). (a) Asymmetric unit of 5IDY. (b) Homotetrameric biologic unit exhibiting dihedral symmetry (D_2). (c) Rotation of (b) to demonstrate symmetry.



Figure 2: Electrostatics and inter-chain interactions. (a) Electrostatic surface of 5IDY chain A with NADP⁺ bound. (b)(c) Illustration of the hydrophobic (blue) and hydrophilic (red) residues along the monomer interfaces. (c) Vertical and horizontal interfaces, rotated 90°, show the hydrophobic residues along the interaction area.



Figure 3: Structural alignment of chain A (blue) from 5IDX to homologs identified using DALI. Homologous structures are shown as listed: 3AI2-D (red) is a NADP sorbose reductase from *Glucoronobacter frateurii* (RMSD = 1.160, 1230 atoms), 1O5I-C (orange) is a 3-oxoacyl-ACP reductase from *Thermotoga maritima* (RMSD = 0.795, 1156 atoms), 3U4C-A (yellow) is a Bacilysin biosynthesis oxidoreductase from *Bacillus subtilis* (RMSD = 1.152, 1243 atoms), 2Q2W-C (forest) is a β -D-hydroxybutyrate dehydrogenase from *Pseudomonas putida* (RMSD = 1.235, 886 atoms) (Kubota *et al.*, 2011) (JCSG, 2003) (Rajavel, 2013) (Paithankar, 2007).

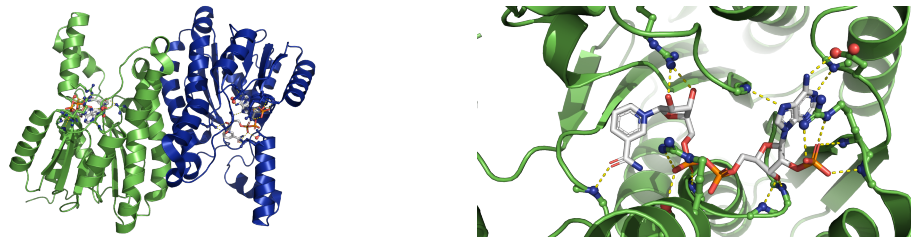


Figure 4: Conformational changes between 5IDX (apo) and 5IDY (NADP⁺ bound). (a) Structural alignment of chain A of 5IDX (lightblue) and 5IDY (blue). (b) Conformation changes (>1 Å, red) of side chain and backbone atoms involved in NADP⁺ (red) binding.

Figure 5: Protein-ligand interactions between 5IDY and NADP⁺. (a) Chain B (green) detailing hydrogen bonds (yellow, 2.7-3.3 Å) between the backbone and side chains of 5IDY and NADP⁺. Electrostatic surface of chain B modeled with (b) NADP⁺ bound and (c) NAD⁺ bound.